Here we provide details about the Aura TES water vapour isotopologue observations and the isotopic model used to interpret those observations. Sections 1 – 3 provide details about the Aura Tropospheric Emission Spectrometer and a summary of the optimal estimation algorithm used for obtaining vertical profiles of HDO and H_2O, characterizing the errors of these profiles, and correcting for a bias in the profiles that is due to spectroscopic error. Section 4 provides a derivation and specific details about the isotopic model used to interpret the TES isotopic vapour observations. In particular, supplemental Figure 2 shows how the family of isotopic models described in the main text vary if different hydrological processes are included (or removed) from the model.

1. Overview of the Tropospheric Emission Spectrometer

The Tropospheric Emission Spectrometer (TES)[1] launched on July, 2004 on the EOS Aura mission provides a global view of tropospheric trace gas profiles including ozone, water vapor, HDO, carbon monoxide along with profiles of atmospheric temperature, surface temperature, surface emissivity and effective cloud parameters (effective cloud height and optical depth) that characterize the physical state[2,3,4,5]. This sets of observations are important to global air quality, climate, and for this study, the hydrological cycle.

TES is an infrared, high resolution, Fourier transform spectrometer covering the spectral range between 650 to 3050 cm^{-1} (3.3 to 15.4 microns) at an apodized spectral resolution of 0.1 cm^{-1} for the downward looking (or nadir viewing) or 0.025 cm^{-1} (limb viewing). The TES nadir spectral resolution was chosen to match the half-width of pressure broadened lines in the boundary layer[1]. Radiances are calibrated using onboard blackbodies; the accuracy of this calibration is approximately 0.3 K[6].

Spectral radiances measured by TES are used to infer the atmospheric state parameters described using a maximum *a posteriori* optimal estimation algorithm that minimizes the difference between these radiances and the equation of radiative transfer subject to the constraint that the parameters are consistent with an statistical a priori description of the atmosphere[7,8]. A critical outcome of this process is a detailed characterization of the smoothing, random, and systematic errors for the estimated atmospheric parameters along with important retrieval metrics such as degrees of freedom and vertical resolution. This inference is possible because individual spectral lines are sensitive to variations in trace gas concentrations at different altitudes.

2. Optimal Estimation of HDO and H2O Profiles

The relationship between the observed spectral radiances and the atmospheric state parameters is described by the additive noise model

$$\mathbf{y} = \mathbf{L}(\mathbf{x}, \mathbf{b}) + \mathbf{n} \tag{2.1}$$

where $\mathbf{y} \in \mathbb{R}^N$ is the observation vector containing in this case the calibrated radiances from TES. The forward model operator, $\mathbf{L} : \mathbb{R}^M \to \mathbb{R}^N$, simulates a spectrum produced from the propagation of radiation through the atmosphere to the spacecraft. The vector $\mathbf{n} \in \mathbb{R}^N$ accounts for white Gaussian noise with a zero-mean. The forward model is evaluated by the atmospheric state vector, $\mathbf{x} \in \mathbb{R}^M$. In this study we define the full state vector $\mathbf{x}$ as the logarithm of the volume mixing ratio (vmr) of HDO (defined as q_D) and H_2O (defined as q_H) as a function of log pressure grid (p) . The vector $\mathbf{b} \in \mathbb{R}^J$ contains all the other parameters, trace gases, atmospheric temperature distribution, geometry of the spacecraft, calibration, etc., necessary to define the radiance for the TES sensors.

The Euclidean norm of the difference of the observed spectral radiances and the forward model is minimized with respect to the atmospheric state subject to the *a priori* statistical distribution of that atmospheric state. If the difference between estimated state, denoted as $\hat{\mathbf{x}} \in \mathbb{R}^M$, and the actual atmospheric state, $\mathbf{x}$, is linear with respect to the spectral radiances, then the estimated state can be written as[5,8]

$$\hat{\mathbf{x}} = \mathbf{x}_a + \mathbf{A}_{xx}(\mathbf{x} - \mathbf{x}_a) + \mathbf{G}\mathbf{n} + \mathbf{G}\sum_i \mathbf{K}_i(\mathbf{b}_i - \mathbf{b}_i^a) \tag{2.2}$$

where $\mathbf{x}_a \in \mathbb{R}^M$ is the *a priori* mean atmospheric state, $\mathbf{n}$ is the noise vector described in (2.1), $\mathbf{b}_j$ is the j^{th} forward model state parameter, and $\mathbf{b}_j^a$ is the mean vector for that forward model parameter. Each of these vectors is transformed to the estimated state by matrices that incorporate information about the radiative transfer and *a priori* information of the atmospheric state. The averaging kernel, $\mathbf{A}_{xx} : \mathbb{R}^M \to \mathbb{R}^M$, smoothes the retrieved estimate of the atmospheric state and accounts for the unresolved fine structure in the atmosphere. The gain matrix, $\mathbf{G} : \mathbb{R}^N \to \mathbb{R}^M$ is the sensitivity of the estimated state to spectral variability, e.g., noise, and the Jacobian, $\mathbf{K}_i : \mathbb{R}^J \to \mathbb{R}^M$, is the sensitivity of the spectral radiances to variations to the j^{th} forward model parameter (e.g., cloud optical depth).

The error in the estimated state

$$\tilde{\mathbf{x}} = \mathbf{x} - \hat{\mathbf{x}} \tag{2.3}$$

can be expanded to

$$\tilde{\mathbf{x}} = \underbrace{\left(\mathbf{I} - \mathbf{A}_{xx}\right)\left(\mathbf{x} - \mathbf{x}_a\right)}_{\text{smoothing error}} + \underbrace{\mathbf{G}\,\mathbf{n}}_{\text{retrieval noise error}} + \underbrace{\mathbf{G}\sum_{\mathrm{j}} \mathbf{K}_j(\mathbf{b}_j - \mathbf{b}_j^a)}_{\text{model error}} \tag{2.4}$$

This error is composed of three terms: smoothing error, retrieval measurement error, and model errors. The smoothing error resulting from selection of the averaging kernel accounts for unresolved structure in the estimate, the measurement error accounts for the spectral measurement noise in the data, and the modeling error accounts for non-retrieved quantities in the forward model such as atmospheric temperature and emissivity over land. The mean and covariance of these terms are the principle measurements of the accuracy and precision of the estimate.

The calculation of the isotopic composition is derived from the ratio between simultaneous estimates of HDO and H_2O:

$$\hat{\mathbf{x}}_R = \log\frac{\hat{q}_D}{\hat{q}_H} = \hat{\mathbf{x}}_D - \hat{\mathbf{x}}_H \tag{2.5}$$

The covariance of the error between the estimated ratio and the true ratio

$$\tilde{\mathbf{x}}_R = \mathbf{x}_R - \hat{\mathbf{x}}_R \tag{2.6}$$

may be derived from (2.4)[5] as

$$\mathbf{S}_R = E[(\tilde{\mathbf{x}}_R - \bar{\tilde{\mathbf{x}}}_R)(\tilde{\mathbf{x}}_R - \bar{\tilde{\mathbf{x}}}_R)^T] = \mathbf{S}_{sm} + \mathbf{S}_n + \mathbf{S}_m \tag{2.7}$$

where the atmospheric state, spectral noise, and model errors are assumed to be uncorrelated.

3. Biases and Data Quality

3.1 Bias Correction

A bias in the established HDO spectroscopic line strengths requires a correction of at least 5% in order for the distribution of TES δD measurements to be consistent with recent air-craft measurements of the HDO/H_2O ratio taken during the Costa Rica Aura

Validation Experiment (http://cloud1.arc.nasa.gov/ave-costarica2/), with recent comparisons of measured thermal infrared HDO spectroscopic line strengths with theoretical work[9], and values simulated by general circulation models. Further validation is offered by examining the TES observed distribution of the HDO/H_2O ratio over ocean where it is expected from simple equilibrium arguments that the isotopic composition cannot exceed -70 ‰[5]. We correct for this bias by using the last term of (2.4):

$$\bar{\hat{\mathbf{x}}}_R \approx \mathbf{G}^D \sum \mathbf{K}^b (\mathbf{b} - \mathbf{b}^a) \tag{2.8}$$

where the term $\mathbf{G}^D$ is a gain matrix that captures the influence of the HDO component on the simultaneous HDO-H_2O retrieval, and the expression $(\mathbf{b} - \mathbf{b}^a)$ is correction to the spectroscopic line strengths. The Jacobian for the spectroscopic line strengths can be shown to be exactly the same as the Jacobian for the (logarithm) of the HDO volume mixing ratio under the assumption that the line strength can be modeled as the product of the absorption coefficient, κ and a scaling factor, β. Then the optical depth for any one of the layers in the forward model atmosphere is given by:

$$\tau_l(\upsilon, p_l) = n_{air} \beta \kappa(\upsilon, P_l) q_D(p_l) \tag{2.9}$$

where υ refers to frequency, p_l refers to the pressure of the layer l, q_D is again the volume mixing ratio of HDO. For a given layer l, β and q_D are a function neither of frequency nor pressure. Consequently,

$$\frac{\partial \mathbf{L}(\upsilon)}{\partial q_l} = \frac{\partial \mathbf{L}(\upsilon)}{\partial \boldsymbol{\tau}_l(\upsilon)} \frac{\partial \boldsymbol{\tau}_l(\upsilon)}{\partial q_l} = \frac{\partial \mathbf{L}(\upsilon)}{\partial \boldsymbol{\tau}_l(\upsilon)} \frac{\partial \boldsymbol{\tau}_l(\upsilon)}{\partial \beta} = \frac{\partial \mathbf{L}(\upsilon)}{\partial \beta} \tag{2.10}$$

The equality condition in (2.10) results in the same matrix **K** that is used for the profile retrieval of HDO and H_2O. Matrix multiplying the Gain matrix in (2.8) by this matrix results in the averaging kernel matrix for HDO. These terms can be used to conveniently evaluate (2.8) where we have assumed that the scaling factor is $\beta = .95$ corresponding to a decrease in the line strength of 5%. Based on this scaling the model correction term for (2.8) is $(\mathbf{b} - \mathbf{b}^a) = \ln(0.95)$.

3.2 Data Selection

The problem of estimating atmospheric profiles from infrared radiances is nonlinear and therefore it is possible for a solution to converge to an unacceptable or unphysical solution for which the error characterization no longer applies. We use a number of criteria to determine if the solution is unacceptable. Many of these criteria are standard and described in the TES data-users guide (available from the Earth Observing System (EOS) Data Gateway:
(http://eosweb.larc.nasa.gov/PRODOCS/tes/table_tes.html).

For the analysis presented here, additional criteria are used for selecting data[5]. We require selection of retrievals that have (1) converged (i.e., the difference between the forward model and observed radiance is comparable to the NESR); (2) the estimate for water is within the expected uncertainty of the estimate from the initial retrieval of temperature and water, and (3) the estimated HDO/H_2O ratio is found to be sufficiently sensitive to the actual distribution of the HDO/H_2O ratio[5]. This last criteria is met by using those observations in which the retrieval degrees of freedom of the HDO component of the profile retrieval is 0.5 or higher; this ensures that the estimate of profile of HDO/H_2O is sufficiently sensitive to the true distribution of HDO/H_2O and that there is significant error reduction in the estimate of the HDO/H_2O ratio relative to the assumed *a priori* covariance[5].

Incorrectly estimating surface emissivity can have a substantial effect on our atmospheric profile retrievals. We therefore remove those observations in which the estimated surface emissivity is substantially different from our *a priori* emissivity, i.e., if the average RMS difference between the estimated and *a priori* emissivity is larger than 3%. Furthermore, we have also found that strong atmospheric emission layers, that is, where the atmospheric temperature in the boundary layer is much larger than the surface temperature, can lead to unphysical solutions; these observations are also removed from our analysis.

4. Review and derivation of simple isotope models

To provide theoretical guidance for the interpretation of isotope observations, we seek an expression for the isotopic composition of atmospheric vapour as a function of water vapour volume mixing ratio. The normalized isotope ratio is given as $R = q_D/(R_{std}q_H)$, where the normalization is by the standard ratio R_{std}, which is typically the value for Vienna Standard Mean Ocean Water ($R_{\mathrm{std}} = 3.11 \times 10^{-4}$ HDO molecules relative to the number of H_2O molecules). As such, we define "delta" as $\delta = \ln R$, and an "approximate delta" as $\delta = R - 1$, where it is conventional to express δ in parts per mil (permil, ‰). To simplify notation, we suppress the subscript H so that q refers to H_2O for the rest of this derivation while q_D refers to HDO as expect.

Changes in the isotope ratio can be written in terms of changes in q and $q_D = Rq$ can be written through application of the chain rule for differentiation as:

$$d\ln R = \frac{dR}{R} = \frac{dRq}{Rq} - \frac{dq}{q} \tag{4.1}$$

Given these definitions, we write the generic form of the desired relationship that relates changes in δ to the abundance of the two isotopalogues,

$$\frac{d\ln R}{dq} = \frac{1}{q}\left[\frac{1}{R}\frac{dq_D}{dq} - 1\right]. \tag{4.2}$$

It is shown below that different physical assumptions applied to the water and isotope mass balance can be included conveniently via the derivative on the right. Integration of (4.2), via either analytic or numerical methods, leads to the expression $\delta = \delta(q)$ which traces a trajectory on a δ–q diagram associated with the isotopic influence of particular hydrologic processes. Supplemental Figure 1 shows schematically the mass balance for the water vapor specific humidity (q) in some region of the atmosphere (nominally that observed by TES) as the sum of evaporation from a moist surface (E), condensation (C), convergence of advective fluxes (A), and recovery of vapour by rain evaporation (X). The precipitation is found by continuity (P = C – X) and represents the large-scale sink of atmospheric moisture. General conservation equations for isotopalogues of water are thus written in Eularian form as:

$$\frac{\partial q}{\partial t} = E - P + A \tag{4.3}$$

The challenge therefore is to evaluate terms on the right for H_2O and HDO so as to capture the isotopic signature of the responsible processes and included in (4.2) before integration.

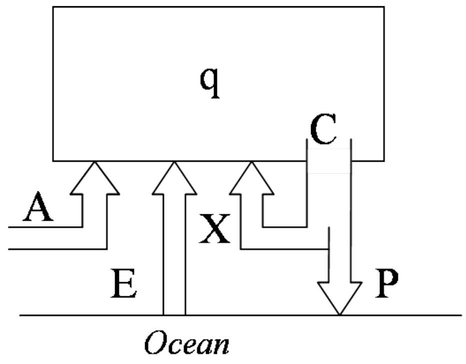

Supplemental Figure 1: Schematic depiction of the atmospheric water budget. Diagram shows changes in the atmosphere reservoir water vapour (q) is the sum of a condensation loss (C), advective convergence (A), evaporation from the surface

(E), and rain evaporation (X) sources. The balance of condensation not evaporated falls as precipitation (P).

4.1 Non-isotopic moisture budgets

We shall assume the advective convergence and precipitation rates are known or otherwise prescribed. We take X to be a constant fraction of the condensation (X = *f*C), which is valid for a fixed relative humidity below the precipitating cloud base. As such, we are left to parameterize the evaporation from the surface in the usual Fickian form[10]

$$E = \gamma(q_s - q) \tag{4.4}$$

where γ is a drag coefficient that captures both molecular and turbulent exchange, and q_s is the saturation mixing ratio for a known surface temperature. Substituting into (4.3), results in a simple first order differential equation,

$$\frac{\partial q}{\partial t} = \gamma(q_s - q) - (1 - f)C + A \tag{4.5}$$

which has the solution

$$q(t) = \hat{q} + (q_0 - \hat{q})e^{-t/\tau}\ . \tag{4.6}$$

This result states that given some initial value, q_0, and knowing the supply of water via A and condensation rate C, the atmospheric water mixing ratio will approach a steady state $\hat{q}$, that is somewhat below saturation, with an e-folding time of $\tau = \gamma^{-1}$ given by

$$\hat{q} = q_s + \frac{1}{\gamma}\left[A - (1 - f)C\right] \tag{4.7}$$

From this solution, the relative importance of precipitation and advection is found quantitatively as the ratio between the quantities P/γ and A/γ, which characterizes the balance between the rate at which each process acts relative to the e-folding timescale required for evaporation to saturate the air.

4.2 General budget models for minor isotopes

From the derivation above, it is clear that minor heavy stable isotopic species are subject to the same budget requirements, with the exception that evaporation is more efficient for lighter nuclides, and condensation more efficient for heavy nuclides. Isotopic fractionation can be captured during evaporation by assuming the vapour at the ocean surface is in isotopic equilibrium with ocean water such that

$$E_D = \gamma\eta\left(R_s q_s - q_D\right) \tag{4.8}$$

At the ocean surface the vapour is taken as $R_s = R_{ocean}/\alpha_s$, where α_s is the equilibrium fractionation at the temperature of the ocean. Kinetic isotope effects are accounted for through the coefficient η which is slightly less than unity and gives a kinetic fractionation of typically -5‰[11]. For condensation it is conventional to assume the condensed phase instantaneously in isotopic equilibrium with the vapour given a fractionation α_c:

$$C_D = \alpha_c CR \tag{4.9}$$

For evaporation of falling liquid condensate a number of assumptions can be made depending on the size, phase and habit of precipitation. We assume that water evaporating from large raindrops (such as associated with vigorous convective systems) is depleted with respect to the liquid, given by an effective fractionation α_e:

$$X_D = \frac{1}{\alpha_e}\frac{C_D}{C}X = \frac{\alpha_c}{\alpha_e} fRC \tag{4.10}$$

This assumption is unlikely to be valid when either raindrops are small and can achieve complete isotopic equilibration with the ambient vapour (such as for stratiform cloud), or the precipitation is solid. The fractionation factors α_c and α_e account for both the thermodynamic equilibrium fractionation and kinetic effects (i.e., diffusion limitation) under non-equilibrium conditions, which acts to decrease fractionation efficiency. More specifically, the term α_e accounts for molecular diffusive transport within raindrops, and through the drop boundary layer[12].

Assigning the isotopic composition of advected vapour as $\overline{R}$, synthesis of all terms into a single budget for q_D, analogous to (4.3) yields:

$$\frac{\partial q_D}{\partial t} = D\eta\left(R_s q_s - q_D\right) - \alpha_c RC\left(1 - \frac{f}{\alpha_e}\right) + \overline{R}A\,. \tag{4.11}$$

Notice the second term on the right is the isotopic composition of precipitation and simply the difference between (4.10) and (4.9). Equation (4.11) is again a first order equation, although now not simple due to the varying coefficient $q = q(t)$ that appears via R. Nonetheless, the steady state can be found as

$$\hat{q}_D = \left(\gamma\eta R_s q_s + \overline{R}A\right)\left[\gamma\eta + \alpha_c \frac{C}{\hat{q}}\left(1 - \frac{f}{\alpha_e}\right)\right]^{-1} \tag{4.12}$$

While obtaining a similar equation in δ notation is straight forward, it is computationally more convenient to solve (4.12) directly and determine δ value as a final step.

4.3 Application of simple models

We consider four limiting cases which are used to explain TES observations of water vapour. Inserting Equations (4.5) and (4.11) into Equation (4.2) we can write a general equation in approximate delta notation which is readily solved numerically to examine behavior of isotope models derived above. However, simpler model configurations that characterize end-member cases are particularly enlightening. In particular, should the initial water vapour and isotopic mixing ratio be known and subject only to condensation (i.e., ignore *E*, *X*, and *A*) the familiar Raleigh distillation is recovered as,

$$\frac{\partial \delta}{\partial q} = \frac{1}{q}(\alpha_c - 1). \tag{4.13}$$

which may be integrated between the initial and final states (q_0, δ_0) and (q, δ). The temperature dependent fractionation factor α_c defines the exponential curvature of the path plotted on a δ-q diagram.

Supplemental Fig. 2a shows the behavior of this model for a range of α_c that encompass values typically seen in the atmosphere (from -20 to 20ºC). This is the simplest description of the isotopic evolution under conditions where water is lost from the atmosphere by condensation.

Should some fraction of falling rain be evaporated and recovered by the air parcel ($X=fC$), a modified Rayleigh model is obtained where isotopic depletion is dictated by the composition of precipitation sink as,

$$\frac{\partial \delta}{\partial q} = \frac{1}{q}\left[\alpha_c\left(\frac{1 - f/\alpha_e}{1 - f}\right) - 1\right] \tag{4.14}$$

Supplemental Fig. 2b shows this model increases the isotopic depletion of the air parcel as water is lost from the atmosphere since the evaporation below the cloud base tends to further enrich the precipitation. As such this model provides a plausible explanation for the amount effect. In the limiting case where all falling condensate is evaporated ($f \to 1$) this model is non-physical. In such a case, one might instead consider the so-called closed equilibrium model in which clouds liquid remains in equilibrium with the vapour[13].

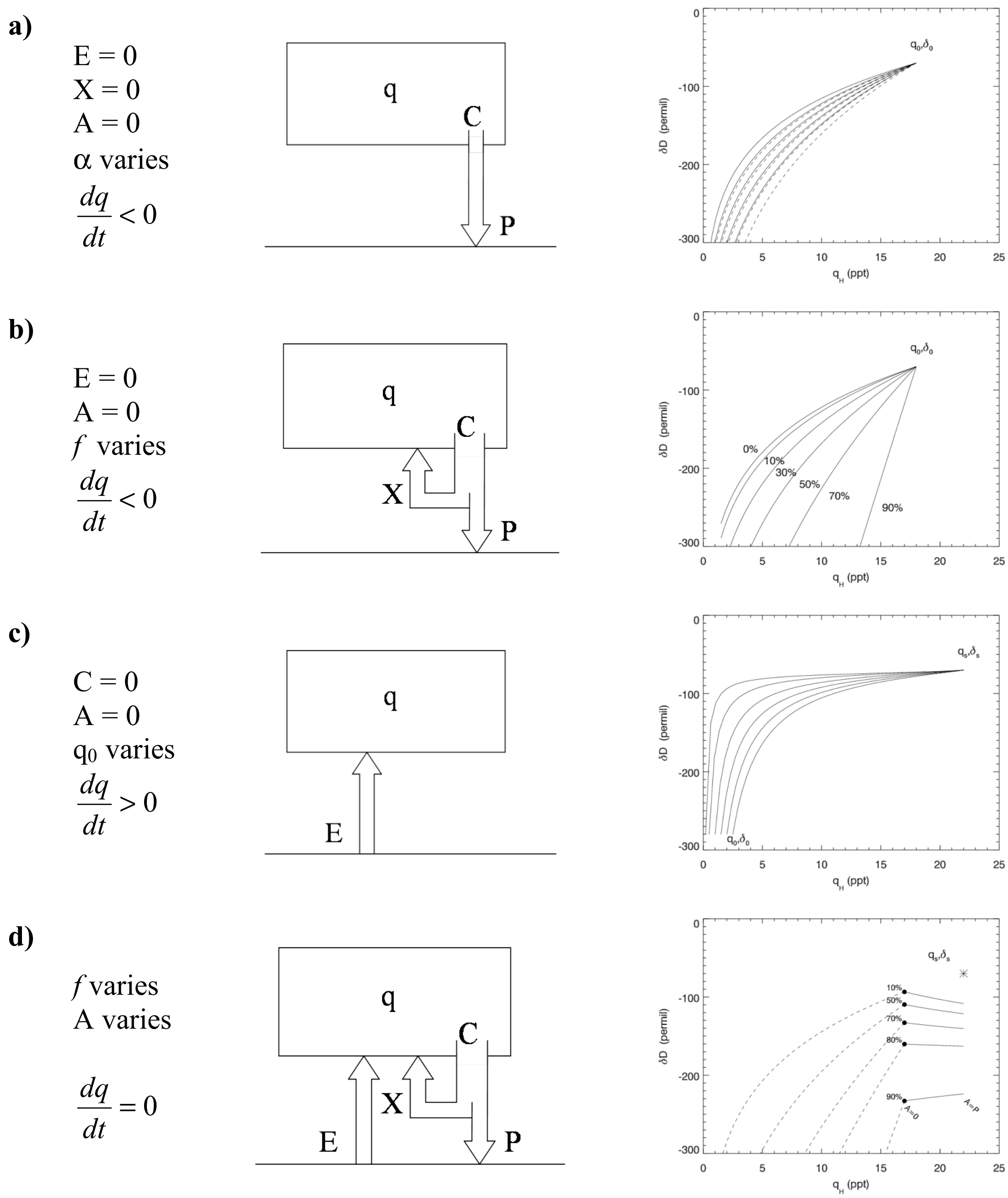

Supplemental Figure 2: Simplified versions of general isotope model as used to defined process curves. The origin of q = 12 ppt, and δ = -70 ‰ is chosen as characteristic for the atmosphere but is arbitrary in demonstrating the differences in the behaviour of the models. The Rayleigh model (a) is linear in ln *q* and is plotted for condensation temperatures of -20, -10, 0, 10, and 20ºC for fractionation to liquid (solid) and ice (dashed). The modified Rayleigh model assumes a condensation temperature of 15ºC and an evaporation temperature of 5ºC. The evaloration curves (c) are linear in 1/q and plotted for a selection of initial points. See text for further details.

While valid also for within individual clouds and where precipitation forms from mechanical coalescence of smaller droplets, a closed system model is not an accurate description of a system in which precipitation reflects continual deposition of vapour as is more likely in tropical cloud systems[13]. Nonetheless, inclusion of cloud liquid with the closed equilibrium assumption in the family of models developed here is straight forward, and acts to bias the isotopic composition of the vapour toward lighter values since the cloud water is enriched relative to the vapour. Since the mass of water stored in clouds liquid is small relative to the mass in vapour phase, this effect is small for all but polar conditions[14]. The cloud water reservoir is nonetheless important in comprehensive isotope schemes used in global climate models where more specific information on the isotopic composition of clouds at all locations is needed.

The gain of water via evaporation in the absence of additional sources or sinks (i.e., C, X and A omitted) can be expressed as a "mixing" model between some initial state, and some infinite reservoir associated with the vapour in equilibrium with, and supplied from, ocean water:

$$\frac{\partial \delta}{\partial q} = \frac{1}{h} \frac{(\delta_s' - \delta) + \varepsilon_s}{(q_s - q)} . \tag{4.15}$$

Since the temperature of the ocean uniquely determines both the saturation vapour volume mixing ratio and, given knowledge of the kinetic effects, $\varepsilon_s = h(1-\eta)$, and the isotopic composition of that vapour δ_s', the trajectory in a δ-q diagram is determined via integration from initial point (q_0, δ_0) to the known surface point (q_s, δ_s), as shown in Supplemental Fig. 2c. Notice importantly the these evaporation curves are more strongly concave down compared to the condensation curves of the Rayleigh model – a feature which allows separation of evaporations and condensation processes via analysis of isotopic observations.

In considering an atmosphere at steady state, as given by (4.7) and (4.12), the supply of water (via evaporation, rain evaporation and advection) must balance the ultimate loss of water by precipitation. Supplemental Fig. 2d shows as solid dots the steady state solution for different values of the rainfall evaporation fraction *f*. Given that *C* and *A* are assumed fixed, *E* adjusts to reach the required balance, which in turn constrains the isotopic budget in view of the prescribed isotopic physics. The role of advection is shown by varying the advective fraction of the total water supply from zero to the entire precipitation flux (*A*=*P*), and shown as solid curves. The isotopic composition is assumed to be the global mass weighted value from the TES observations of $\overline{\delta}$ = -180‰, and the advection acts to bias the evolution of the system toward this isotopic composition at a rate determined by the magnitude of the advective flux relative to the evaporative supply (as noted above). To close the budget calculations we select characteristic values of γ=0.2 day^{-1} and P = 1 day $^{-1}$ (about 5 mm day^{-1} of rain). While these choices influence the details of the model, the characteristic behavior is robust. If, however, the model is applied to a region of sufficient size or in which moist processes are rapid relative to the advective time scale, the advective supply can by largely neglected and this term vanishes. Should, evaporation stop, again the modified Rayleigh model results (as in Supplemental Fig. 2b) but now the initial point is lower on the δ-q diagram. This provides an additional mechanism for which the amount effect seen in observational data can be explained.

In this family of isotope models, selection of the fractionation parameters and assignment of the advection and condensation rates changes the details of the resulting δ-q curves. While the data and physical reasoning allows the range of values for these to be somewhat constrained, they are not well know from *a priori* estimates. As such, one utility of the isotopic analysis is that these parameters which are fundamental to the water cycling can be constrained further. Moreover, for all models discussed here, explicit information on rates is lost and it emerges that it is the relative magnitude of all contributing fluxes that is important. On the δ-q diagram rates determine speed along a trajectory while the shape of the trajectory itself is determined by the isotopic exchange characteristics of the processes. As such, these curves guide the interpretation of observations rather than provide unambiguous quantification of processes.

References

1. Beer, R., Glavich, T. A. & Rider, D. M. Tropospheric emission spectrometer for the Earth Observing System's Aura Satellite. Applied Optics 40, 2356-2367 (2001).

2. Bowman, K. W. et al. Capturing time and vertical variability of tropospheric ozone: A study using TES nadir retrievals. Journal of Geophysical Research-Atmospheres 107, 4723-4734 (2002).

3. Worden, J. et al. Predicted errors of tropospheric emission spectrometer nadir retrievals from spectral window selection. Journal of Geophysical Research-Atmospheres 109, 4522 - 4534 (2004).

4. Kulawik, S. et al. Implementation of cloud retrievals for Tropospheric Emission Spectrometer (TES) atmospheric retrievals - part I description and characterization of errors on trace gas retrievals. Journal of Geophysical Research-Atmospheres, In Press, (2006).

5. Worden, J *et al.* TES observations of the tropospheric HDO/H_2O Ratio: estimation approach and characterization**.** Journal of Geophysical Research-Atmospheres, In Press, (2006).

6. Worden, H. et al. TES level 1 algorithms: Interferogram processing, geolocation,

radiometric, and spectral calibration. IEEE Transactions on Geoscience and Remote Sensing 44, 1288-1296 (2006).

7. Rodgers, C. D. Inverse methods for atmospheric sounding : theory and practice (World Scientific, Singapore ; London, 2000).

8. Bowman, K. W. et al. Tropospheric emission spectrometer: Retrieval method and error analysis. IEEE Transactions on Geoscience and Remote Sensing 44, 1297-1307 (2006).

9. Voronin, B.A., R.N. Tolchenov, and J. Tennyson Analysis of the accuracy of line positions and intensities of HDO transitions in HITRAN2004, Proceedings from The 9th HITRAN Database Conference, Harvard-Smithsonian Center for Astrophysics, Cambridge, MA, USA, June 26-28, 2006.

10. Noone, D. & Simmonds, I. Associations between delta O-18 of water and climate parameters in a simulation of atmospheric circulation for 1979-95. Journal of Climate 15, 3150-3169 (2002).

11. Merlivat, L. & Jouzel, J. Global climatic interpretation of the deuterium-oxygen-18 relationship for precipitation. J. Geophys. Res. 84, 5029-5033 (1979).

12. Stewart, M. K. Stable isotope fractionation due to evaporation and isotopic exchange of falling waterdrops: Applications to atmospheric processes and evaporation of lakes. J.

Geophys. Res. 80, 1133-1146 (1975).

13. Jouzel, J. Isotopes in cloud physics: multistep and multistage processes in Handbook of environmental isotope geochemistry, vol.2, The terrestrial environment B (eds. Fritz, P. & Frontes, J. C.) 61-112 (Elsevier, New York, 1986).

14. Ciais, P. & Jouzel, J. Deuterium and oxygen 18 in precipitation: an isotopic model including mixed cloud processes. J. Geophys. Res. 99, 19783-16803 (1994).